Journal of Alloys and Compounds 509 (2011) 5913–5918

Contents lists available at ScienceDirect

Journal of Alloys and Compounds

journal homepage: www.elsevier.com/locate/jallcom

Synthesis and characterization of $La_2Ti_2O_7$ employed for photocatalytic degradation of reactive red 22 dyestuff in aqueous solution

Wei-Ming Hou, Young Ku*

Department of Chemical Engineering, National Taiwan University of Science and Technology, 43, Keelung Road, Section 4, Taipei 106, Taiwan

ARTICLE INFO

Article history:
Received 23 December 2010
Received in revised form 3 March 2011
Accepted 4 March 2011

Keywords:
$La_2Ti_2O_7$
Photocatalysis
Perovskite
Polymerized complex method
Reactive Red 22

ABSTRACT

Perovskite structured $La_2Ti_2O_7$ catalyst prepared by polymerized complex method was characterized and examined the photocatalytic activity by decomposing an azo dyestuff, Reactive Red 22, in aqueous solutions under UV irradiation. $La_2Ti_2O_7$ powders prepared by polymerized complex method exhibit higher surface areas, better homogeneity and are more sensitive to solution than those prepared by solid-state method. The first derivatives of UV–vis DRS patterns confirmed the complete crystallization of $La_2Ti_2O_7$ sintered at temperatures higher than 900 °C. The effects of sintering temperature of catalyst and solution pH of photocatalytic reaction were studied. The photocatalytic decomposition of Reactive Red 22 per unit surface area was found to be higher for experiments using $La_2Ti_2O_7$ than using TiO_2. However, the electron–hole recombination was found to be more obvious for $La_2Ti_2O_7$ than for TiO_2 because the network of metal cations constructed within $La_2Ti_2O_7$ enhances the mobility of photogenerated electrons and holes.

1. Introduction

Photocatalytic processes have lately attracted numerous researches in the area of wastewater treatment, especially for treating wastewater containing traces of toxic organic substances. A range of photocatalysts were fabricated and studied extensively in decomposing different organic contaminants. However, the rapid recombination of photogenerated electron–hole pairs critically limits the effectiveness of photocatalytic processes. Recently, several new perovskite structured photocatalysts with highly donor-doped layered structures have been found to be competent on photocatalytic applications, including water-splitting [1–3], Cr(VI) reduction [4], NO oxidation [5] and decomposition of organic compounds [6,7]. Perovskites contains a cubic structure with three different ions, as form of ABO_3 [8]. A series of perovskite structured photocatalysts, such as $LaNiO_3$ [7], $Bi_4Ti_3O_{12}$ [9,10], $Bi_2Zn_{2/3-x}Cu_xTa_{4/3}O_7$ [11], $BiVO_4$ [12] and $La_2Ti_2O_7$ [6], have been investigated over their photocatalytic properties and applications. The separation of electrons and holes in the perovskites is easier than that in other semiconductor materials because of their narrower depletion layers.

$La_2Ti_2O_7$ is a layer-structured perovskite that the photogenerated electrons possess enough energy to promote hydrogen production [13,14]. Hwang et al. [15] synthesized various perovskite structured catalysts, including $La_2Ti_2O_7$, $La_4CaTi_5O_{17}$ and $Sr_2Nb_2O_7$, for photocatalytic water-splitting under UV irradiation, the quantum yields (12–23%) of these catalysts were reported to be much higher than that (<1%) of TiO_2. Abe et al. [2] reported that the high photocatalytic water-splitting activity of these perovskite structured catalysts could be attributed to their octahedral structure to enhance the mobility of photogenerated electrons and holes.

Perovskites are usually synthesized by the solid state reaction (SSR) method in which the precursor oxides are mixed by dry- or wet-grinding and then sintered at temperatures higher than 1000 °C, for a long period [16]. However, perovskites generated by this method usually possess less surface area and low crystalline purity that result in inferior photocatalytic activities. Perovskites are also synthesized by the polymerized complex (PC) method, which is carried out by the formation of a polymerization network by condensing ethylene glycol, citric acid and soluble metal precursors [17,18]. PC method is frequently used in synthesizing homogeneous metal-oxide fine powders with higher surface areas and more uniform morphology, due to the well-mixing of metal ions in molecular level and low preparing temperature [2].

In this study, the perovskites $La_2Ti_2O_7$ prepared by PC method and sintered at various temperatures was characterized by a sequence of analyses, including TG–DTA, XRD, BET, UV–vis DRS and Zeta potential. Photocatalytic decomposition of a frequently studied dyestuff, Reactive Red 22 (RR22, molecular structure presented in Fig. 1), in aqueous solutions using prepared $La_2Ti_2O_7$ was studied under various operating conditions and compared with those using commercial P25 TiO_2 and $La_2Ti_2O_7$ prepared by SSR method.

* Corresponding author. Tel.: +886 2 27333141x7606; fax: +886 2 23785535.
E-mail address: ku508@mail.ntust.edu.tw (Y. Ku).

0925-8388/$ – see front matter © 2011 Elsevier B.V. All rights reserved.
doi:10.1016/j.jallcom.2011.03.042

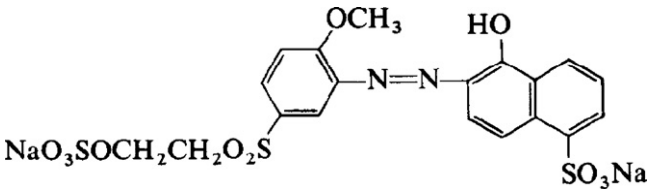

Fig. 1. Molecular structure of Reactive Red 22.

2. Experimental

Titanium isoproxide (TTIP, $Ti(OCH(CH_3)_2)_4$, Acros), ethylene glycol (EG, $C_2H_6O_2$, Acros), citric acid (CA, $C_6H_8O_7$, Acros) and lanthanum nitrate hydrate ($La(NO_3)_3{\cdot}6H_2O$, Acros) were used as starting materials without further purification. Citric acid was used as the metal chelating agent and ethylene glycol as the polyol [16]. After dissolving 0.1 mol of TTIP in 4 mol of EG, 1 mol of CA was added to the solution to convert TTIP to stabilize the Ti-citric acid complexes. 0.105 mol of $La(NO_3)_3{\cdot}6H_2O$ was then added to the solution and the mixture was stirred for 1 h at 50 °C until it became transparent. Upon continuous heating at 130 °C for several hours, the solution became highly viscous with a color change to deep brown and, finally, gelled into a transparent-brown glassy resin. Charring the glassy resin at 350 °C for 2 h in a furnace resulted in black powder, which was then grounded into finer powder referred to as the "powder precursor". Thermogravimetry–differential thermal analysis (TG–DTA, PerkinElmer, Diamond TG/DTA) was employed to analyze the pyrolysis of the powder precursor. The black powder was subsequently heated in a crucible at 500–1100 °C for 2 h, followed by cooling to room temperature to form white $La_2Ti_2O_7$ powder. The powder was later characterized by a sequence of analyses, X-ray diffraction (XRD, Regaku, RTP 300RC, Cu Kα radiation of λ = 1.5405 Å), Brunauer–Emmett–Teller approach (BET, Quantachrome, Autosorb-1), UV–vis diffuse reflectance spectroscopy (UV–vis DRS, Jasco, ISV-469), zeta meter (Malvern, S2000) and photoluminescence spectra (PL, Jasco, FP-6500LE).

$La_2Ti_2O_7$ powder was afterward suspended in aqueous solution containing RR22 in a stirred Pyrex reactor (9 cm inter diameter, 25 cm height, 1.65 l volume). All experiments were conducted at 24 ± 1 °C, and the air flow rate entering the photoreactor was kept at 75 ml/min in order to maintain the maximum dissolved oxygen in aqueous solution. The solution pH was kept at desired levels by the additions of sodium hydroxide and/or nitric acid solutions using an automatic titrator. The suspension was put in a dark surrounding for 30 min to achieve adsorption equilibrium before it was irradiated by a pre-warmed 10 W, 254 nm low-pressure mercury lamp with light intensity of 8.35 mW/cm^2. Aliquots of the reaction solution were sampled at intermittent periods of reaction time, and then centrifuged to remove $La_2Ti_2O_7$ particles. Concentration of RR22 in aqueous solutions was measured by the UV–vis spectrometer (Jasco, V-550) at 509 nm.

3. Results and discussion

The TG–DTA result of the $La_2Ti_2O_7$ precursor for a heating rate of 10 °C/min is shown in Fig. 2. The TG curve depicted a significant weight loss at the temperature range from 300 to 500 °C, and a minor weight loss at around 790 °C. The first weight loss is corresponded to the major exothermic peak at 463.5 °C ascribing to the decomposition of most organic compounds contained in the powder precursor. Milanova et al. [16] also prepared $La_2Ti_2O_7$ by PC method, and reported that there was a continuous weight loss below 500 °C. The minor weight loss related to the second exothermic peak at around 792 °C is attributed to the decomposition of residual organics. Kakihana et al. [19] reported that the TG analysis of perovskite $Y_2Ti_2O_7$ showed two obvious weight loss at 550 and 800 °C ascribed to the decomposition of most organics and burnout of residual organics, respectively.

Fig. 3 shows the XRD patterns of $La_2Ti_2O_7$ powders prepared by PC method and sintered at various temperatures for 2 h in the 2θ range of 10–90°. When the samples were sintered at temperatures below 600 °C, the XRD patterns indicated the presence of amorphous solids. The crystallization of $La_2Ti_2O_7$ was observed for samples sintered at temperatures higher than 700 °C. Comparing with JCPDS database (no. 81-1066) of $La_2Ti_2O_7$, the XRD reflections of samples sintered at temperatures above 900 °C exhibited a single phase of $La_2Ti_2O_7$ with a monoclinic structure. From the XRD results, the average crystal size of the $La_2Ti_2O_7$ powders determined from the diffraction peak employing the Scherrer formula. The average crystal size of $La_2Ti_2O_7$ samples was increased from

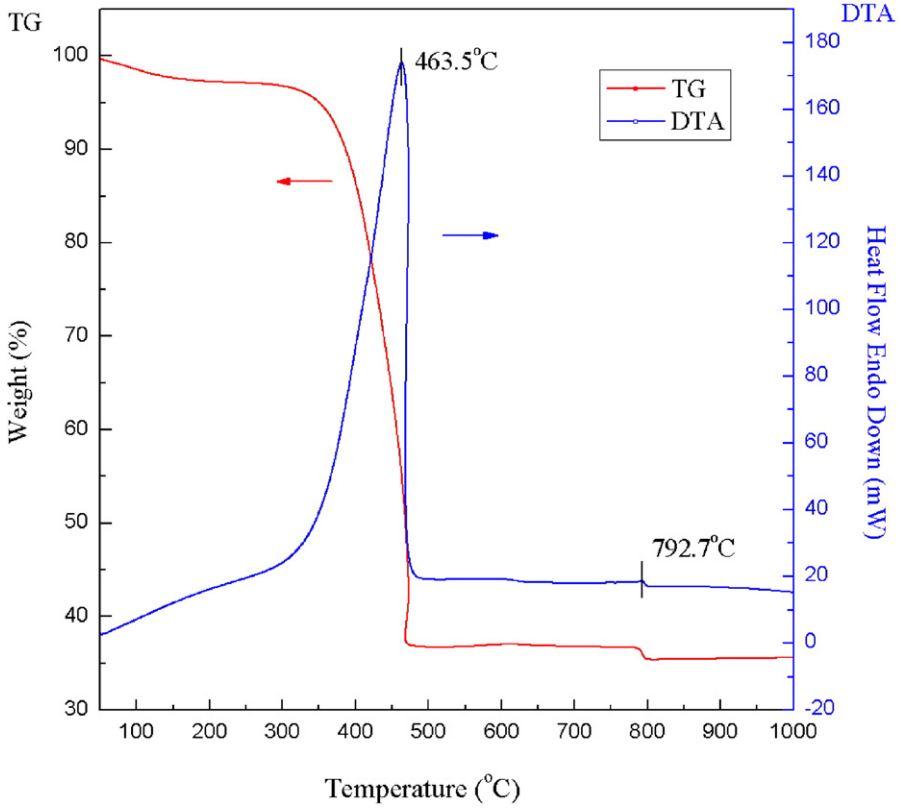

Fig. 2. TG–DTA curves of $La_2Ti_2O_7$ precursor with a heating rate of 10 °C/min.

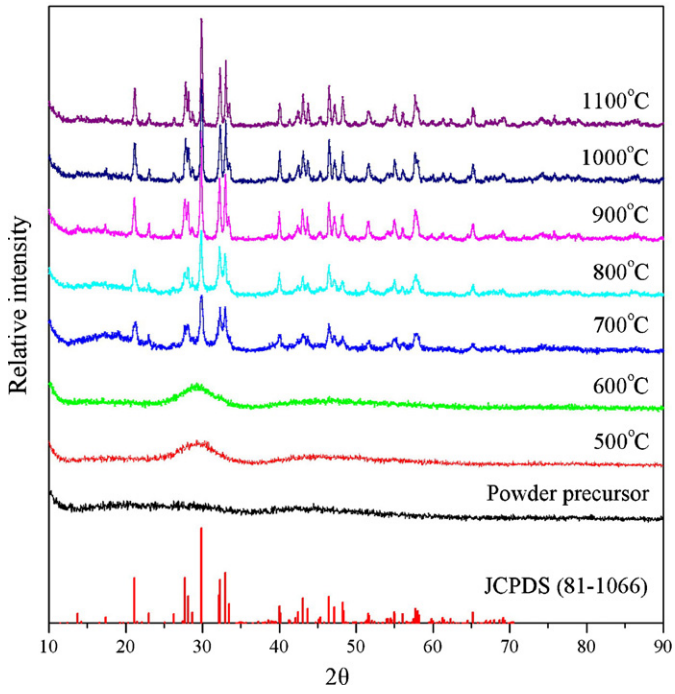

Fig. 3. XRD pattern of $La_2Ti_2O_7$ catalysts sintered at different temperatures and the JCPDS card no. 81-1066.

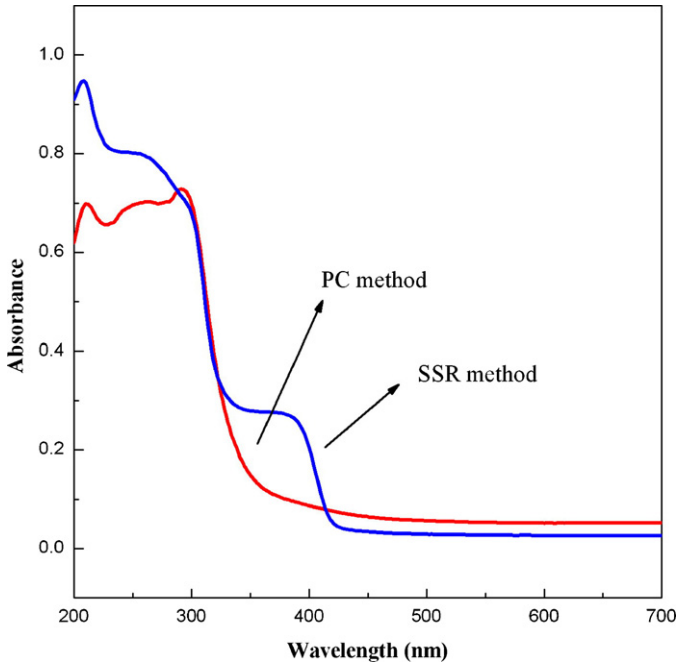

Fig. 5. UV–vis DRS patterns of $La_2Ti_2O_7$ prepared by PC and SSR methods.

35.1 to 42.3 nm with increasing sintering temperature from 900 to 1100 °C, larger than that of commercial P25 TiO_2 (21 nm).

The photocatalytic activity of $La_2Ti_2O_7$ catalysts sintered at various temperatures was examined by decomposing RR22 in neutral solutions with 254 nm UV irradiation and described with apparent first-ordered kinetics because of the relatively low initial RR22 concentration employed in this study [20]. As shown in Fig. 4, only 40–50% of RR22 were decomposed after 3 h of reaction time for experiments conducted with $La_2Ti_2O_7$ catalysts sintered at 500 and 600 °C, even slightly lower than the decomposition of RR22 by photolysis. It is attributed that the amorphous $La_2Ti_2O_7$ sintered at 500 or 600 °C could not be excited by 254 nm UV irradiation, and yet exhibited shielding effect to retard the photolytic decomposition of RR22. However, more then 80% of RR22 were decomposed in the first hour of reaction for experiments using well-crystallized $La_2Ti_2O_7$ sintered at temperatures higher than 700 °C. Based on the experimental results, the $La_2Ti_2O_7$ sintered at 900 °C was chosen to study the subsequent characterization analyses and the photocatalytic decomposition of RR22.

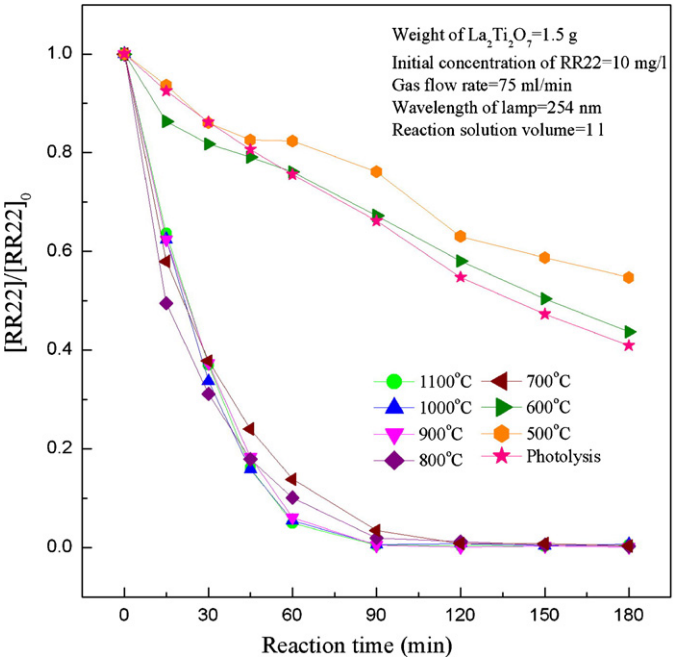

Fig. 4. Effect of $La_2Ti_2O_7$ sintered temperature on photocatalytic degradation of RR22 in neutral aqueous solution.

The UV–vis DRS patterns for $La_2Ti_2O_7$ prepared in this study by PC method was measured in the wavelength range of 200–800 nm, and are compared with the results for $La_2Ti_2O_7$ prepared by SSR method from our previous study [6], as illustrated in Fig. 5. The band gap energy of these two samples was both determined to be 3.55 eV (350 nm) ascribed to a charge transfer from valence band to conduction band. The determined band gap energy of $La_2Ti_2O_7$ was higher than that of commercial P25 TiO_2 (3.1 eV) [20]. Furthermore, a shoulder peak at 435 nm (band gap energy of 2.86 eV) was observed for the sample prepared by SSR method. Kim et al. [21] ascribes the absorption to impurities generated during the course of SSR method, indicating that the $La_2Ti_2O_7$ particles prepared by PC method exhibit better homogeneity than those prepared by SSR method.

The subtle spectral signal can be enhanced to better resolution by the first- or higher-order derivatives of a typical UV–vis spectrum in order to elucidate the unresolved or overlapping bands of multi-component samples [22]. The original and first derivatives of UV–vis DRS patterns for $La_2Ti_2O_7$ sintered at various temperatures are shown in Fig. 6. From Fig. 6(a), there is no obvious relation between the absorbed wavelength and sintering temperature of $La_2Ti_2O_7$. However, as indicated in Fig. 6(b), the first derivatives of UV–vis DRS patterns indicate more complete peaks for $La_2Ti_2O_7$ sintered at temperatures higher than 900 °C, further confirmed the complete crystallization of $La_2Ti_2O_7$ sintered at higher temperatures. The first derivative curves for these $La_2Ti_2O_7$ sintered at temperatures below 800 °C might be attributed to the presence of amorphous $La_2Ti_2O_7$.

The zeta potentials of $La_2Ti_2O_7$ prepared by PC and SSR methods in aqueous solutions of different pH are illustrated in Fig. 7.

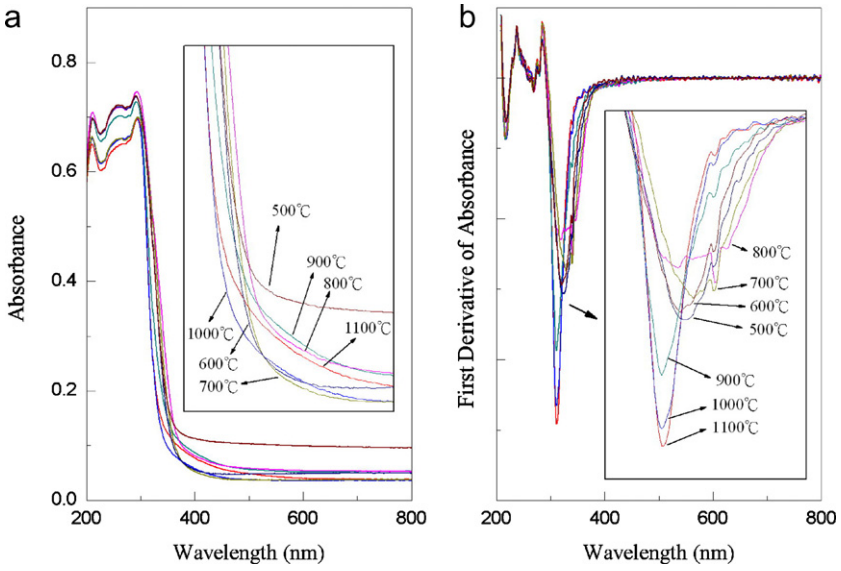

Fig. 6. (a) UV–vis DRS spectra, and (b) the first derivatives of UV–vis DRS, of $La_2Ti_2O_7$ photocatalysts sintered at different temperatures.

Table 1
Photocatalytic decomposition rate constants of RR22 using $La_2Ti_2O_7$ in aqueous solutions of various pH levels.

Solution pH	Reaction rate constant (min^{-1})	R^2
3	0.0954	0.9101
5	0.0648	0.9767
9	0.0426	0.9533
11	0.0625	0.9889

Reaction conditions: $C_{catalysts}$ = 1.5 g/l; sintered temperature of catalysts = 900 °C; C_{RR22} = 10 mg/l; air flow: 75 ml/min; light source = 10 W low-pressure mercury lamp (254 nm); reaction solution volume = 1 l.

Although these $La_2Ti_2O_7$ samples were prepared by different methods, the pH_{zpc} values of both samples were determined to be around 7.2. However, the zeta potential of $La_2Ti_2O_7$ prepared by PC method exhibited more abrupt variation than that prepared by SSR method, indicating that the surface potential of $La_2Ti_2O_7$ prepared by PC method is more sensitive to solution pH. Wang and Ku [23] reported that the pH_{zpc} of P25 TiO_2 was 6.8, slightly lower than that of $La_2Ti_2O_7$. The BET surface area of $La_2Ti_2O_7$ samples prepared by PC and SSR methods were determined to be 8.92 and 3.2 m^2/g, respectively. The surface area of P25 TiO_2 was reported to be roughly 50 m^2/g, much higher than those of prepared $La_2Ti_2O_7$ samples. The adsorption of RR22 by $La_2Ti_2O_7$ prepared by PC and SSR methods in aqueous solutions of various pH levels is depicted in Fig. 8. The Reactive Red 22 is disodium salt and negatively charged in aqueous solution because of the detachment of sodium ions [24,25]. The chemical equation of RR22 dissolved in water is presented as:

$$Dye\text{–}SO_3Na_{(s)} \leftrightarrow Dye\text{–}SO_3^-{}_{(aq)} + Na^+{}_{(aq)}$$

The adsorption of RR22 per unit surface area in acidic solutions by $La_2Ti_2O_7$ prepared using PC method was drastically higher than

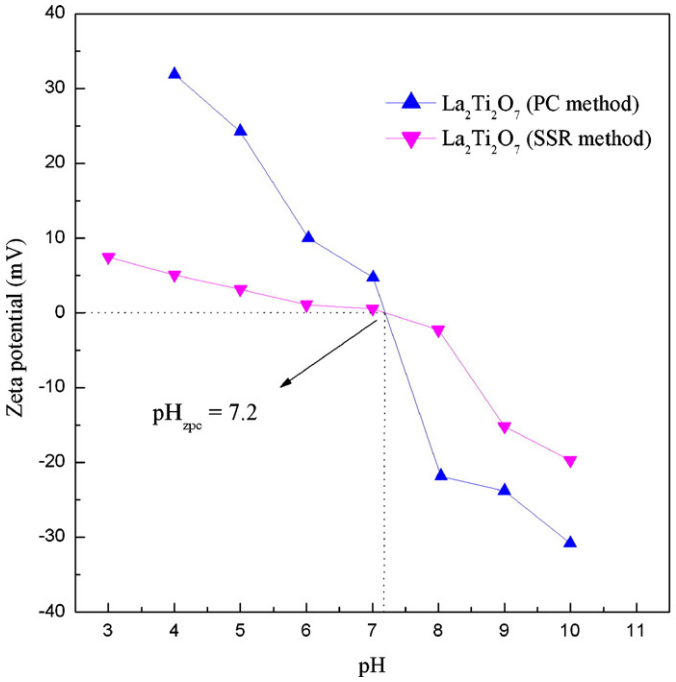

Fig. 7. Determined pH_{zpc} values of $La_2Ti_2O_7$ prepared by PC and SSR methods.

that by $La_2Ti_2O_7$ prepared using SSR method. The adsorption of RR22 in aqueous solution by $La_2Ti_2O_7$ prepared by PC method was considerably influenced by solution pH. However, the adsorption of RR22 by $La_2Ti_2O_7$ prepared by SSR method was slightly varied in solutions of different pH levels. Adsorptions of RR22 by $La_2Ti_2O_7$

Table 2
Comparison of the photocatalytic activities and characterizations of $La_2Ti_2O_7$ and commercial TiO_2 (P25).

Catalyst	Crystal size (nm)	BET (m^2/g)	Reaction rate constant (min^{-1})	Reaction rate constant per unit surface area ($(min\,m^2)^{-1}$)
$La_2Ti_2O_7$	35.1	8.92	0.0257	0.00192
TiO_2 (P25)	21	50	0.1269	0.00159

Reaction conditions: $C_{catalysts}$ = 1.5 g/l; sintered temperature of $La_2Ti_2O_7$ = 900 °C; C_{RR22} = 50 mg/l; air flow: 75 ml/min; solution pH 3; light source = 10 W low-pressure mercury lamp (254 nm); reaction solution volume = 1 l.

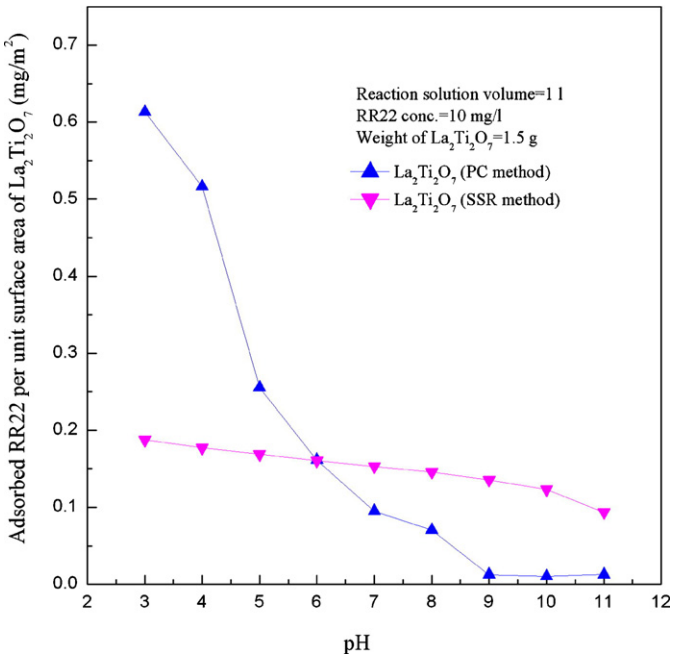

Fig. 8. Adsorption of RR22 by $La_2Ti_2O_7$ catalyst in aqueous solution of various pH levels.

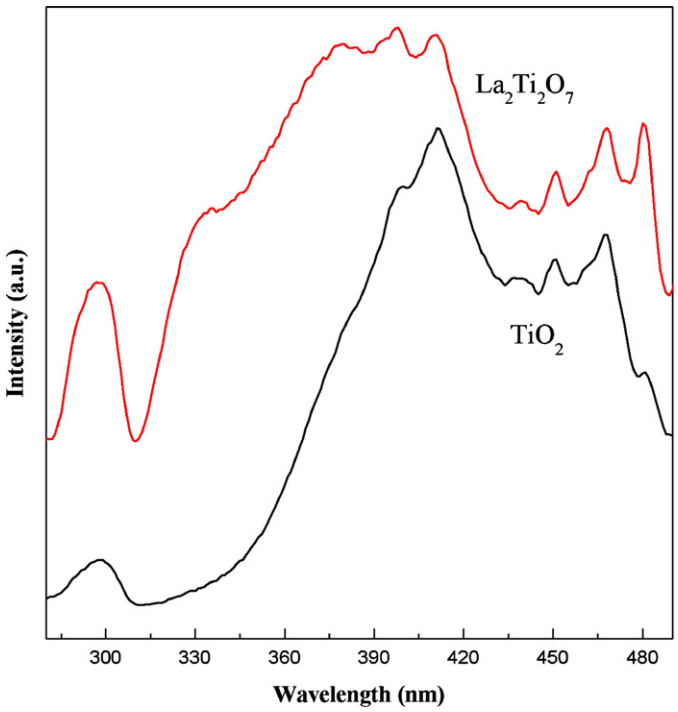

Fig. 9. Photoluminescence spectra of pure $La_2Ti_2O_7$ and TiO_2 with the excitation wavelength of 254 nm.

suspensions were found to be preferred in acidic solutions, and drastically reduced with increasing solution pH levels. These results agree with the observations that the zeta potential of $La_2Ti_2O_7$ is also reduced with increasing solution pH. It is ascribed that the adsorption of RR22 is highly influenced by the surface charge of $La_2Ti_2O_7$ particles.

The first-ordered photocatalytic decomposition rate constants of RR22 in aqueous solutions of different pH level using $La_2Ti_2O_7$ sintered at 900 °C are presented in Table 1. Higher decompositions of RR22 were achieved for experiments carried out in acidic solutions, possibly because the negatively charged RR22 species are adsorbed on the positively charged $La_2Ti_2O_7$ surface, and then decomposed by the photo-induced holes on the surface of $La_2Ti_2O_7$. However, the surface of $La_2Ti_2O_7$ was negatively charged in alkaline solutions, and repulsion occurred between the negatively charged RR22 ions and $La_2Ti_2O_7$ surface to decrease the decomposition of RR22. In alkaline solutions, RR22 is mainly decomposed by the photo-induced hydroxyl radicals generated by excitation of hydroxide ions.

Table 2 shows the comparisons of characterizations and photocatalytic activities between $La_2Ti_2O_7$ and commercial P25 TiO_2. With the same loadings of photocatalyst applied, TiO_2 exhibited higher overall photocatalytic activity than $La_2Ti_2O_7$ in degrading RR22. However, the degradation of RR22 per unit surface area using $La_2Ti_2O_7$ was higher than that using TiO_2. The inferior overall photocatalytic activity of $La_2Ti_2O_7$ is conjectured to its relatively large particle size and low surface area. The perovskite structured $Bi_4Ti_3O_{12}$ prepared by Yao and co-workers [10,26] also exhibited higher photocatalytic activity per unit surface area for decomposing methyl orange than P25 TiO_2, although the overall photocatalytic activity using $Bi_4Ti_3O_{12}$ was lower than that using P25 TiO_2. Therefore, application of synthesis process of lower sintering temperature is advantageous to enhance the surface area and overall photocatalytic activity of $La_2Ti_2O_7$.

The photoluminescence (PL) spectra are widely used to investigate the behavior of electron–hole pairs and efficiency of charge carrier trapping, immigration and transfer [27]. In Fig. 9, the PL spectra of $La_2Ti_2O_7$ and TiO_2 were measured with a 254 nm UV light. The PL intensity of $La_2Ti_2O_7$ was higher than that of TiO_2, indicating the electron–hole recombination for $La_2Ti_2O_7$ was more obvious than that for TiO_2 because the network of metal cations constructed within $La_2Ti_2O_7$ enhances the mobility of photogenerated electrons and holes. Hwang et al. [28] reported that the NiO loading on the surface of $La_2Ti_2O_7$ could efficiently absorb photogenerated electrons and further retard the recombination rate of photogenerated electron–hole. Therefore, additional modifications of $La_2Ti_2O_7$ to capture the photogenerated electrons are beneficial to improve its photocatalytic activity.

4. Conclusions

$La_2Ti_2O_7$ particles prepared by PC method exhibit higher surface areas, better homogeneity and are more sensitive to solution pH than those prepared by SSR method. The crystallization of $La_2Ti_2O_7$ was observed for samples sintered at temperatures higher than 700 °C. The first derivatives of UV–vis DRS patterns confirmed the complete crystallization of $La_2Ti_2O_7$ samples sintered at temperatures higher than 900 °C. The zeta analysis indicated that the surface potential of $La_2Ti_2O_7$ prepared by PC method is more sensitive to solution pH than those prepared by SSR method. The adsorption of RR22 was substantially affected by the surface charge of $La_2Ti_2O_7$ particles. More than 80% of RR22 decomposed in the first hour of reaction for experiments using well-crystallized $La_2Ti_2O_7$. Photocatalytic decomposition of RR22 per unit surface area was found to be higher for experiments using $La_2Ti_2O_7$ than that using TiO_2. However, the poorer overall photocatalytic activity using $La_2Ti_2O_7$ was primarily attributed to its relatively large particle size and low surface area. The network of metal cations constructed within $La_2Ti_2O_7$ enhances the mobility of photogenerated electrons and holes, and then further increases the recombination rate of electron–hole pairs. Therefore, synthesis of $La_2Ti_2O_7$ at lower sintering temperature to enhance the surface area and modifications of $La_2Ti_2O_7$ to reduce the electron–hole recombination are advantageous to improve the photocatalytic activity of $La_2Ti_2O_7$.

Acknowledgement

This research was financially supported by grant NSC-93-2211-E011-014 from the National Science Council, Taiwan, Republic of China.

References

[1] Y. Yang, Q. Chen, Z. Yin, J. Li, J. Alloys Compd. 488 (2009) 364–369.
[2] R. Abe, M. Higashi, K. Sayama, Y. Abe, H. Sugihara, J. Phys. Chem. B 110 (2006) 2219–2226.
[3] Y. Miseki, H. Kato, A. Kudo, Energy Environ. Sci. 2 (2009) 306–314.
[4] Q.L. Yang, S.Z. Kang, H. Chen, W. Bu, J. Mu, Desalination 266 (2011) 149–153.
[5] U. Sulaeman, S. Yin, T. Sato, Appl. Catal. B 102 (2011) 286–290.
[6] Y. Ku, L.C. Wang, C.M. Ma, Chem. Eng. Technol. 30 (2007) 895–900.
[7] Y. Li, S. Yao, W. Wen, L. Xue, Y. Yan, J. Alloys Compd. 491 (2010) 560–564.
[8] Y. Yang, Y.B. Sun, Y.S. Jiang, Mater. Chem. Phys. 96 (2006) 234–239.
[9] G. Zhang, J. Zhou, X. Ding, Y. Hu, J. Xie, J. Hazard. Mater. 158 (2008) 287–292.
[10] W.F. Yao, X.H. Wu, H. Wang, J.R. Zhou, X.N. Yang, Y. Zhang, S.X. Shang, B.B. Huang, Appl. Catal. B 52 (2004) 109–116.
[11] J. Sun, G. Chen, Y. Li, C. Zhou, H. Zhang, J. Alloys Compd. 509 (2011) 1133–1137.
[12] C. Yu, K. Yang, J.C. Yu, F. Cao, X. Li, X. Zhou, J. Alloys Compd., doi:10.1016/j.jallcom.2011.01.100.
[13] A. Kudo, Y. Miseki, Chem. Soc. Rev. 38 (2009) 253–278.
[14] C.C. Hu, H. Teng, Appl. Catal. A 331 (2007) 44–50.
[15] D.W. Hwang, H.G. Kim, J.K. Kim, K.Y. Cha, Y.G. Kim, J.S. Lee, J. Catal. 193 (2000) 40–48.
[16] M.M. Milanova, M. Kakihana, M. Arima, M. Yashima, M. Yoshimura, J. Alloys Compd. 242 (1996) 6–10.
[17] M.P. Pechini, US Patent 3,330,697, July 11 (1967).
[18] H. Wang, R. Zuo, J. Fu, Y. Liu, J. Alloys Compd. 509 (2011) 936–941.
[19] M. Kakihana, M.M. Milanova, M. Arima, T. Okubo, M. Yashima, M. Yoshimura, J. Am. Ceram. Soc. 79 (1996) 1673–1676.
[20] Y.L. Kuo, H.W. Chen, Y. Ku, Thin Solid Films 515 (2007) 3461–3468.
[21] H.G. Kim, D.W. Hwang, S.W. Bae, J.H. Jung, J.S. Lee, Catal. Lett. 91 (2003) 193–198.
[22] C.B. Ojeda, F.S. Rojas, Anal. Chim. Acta 518 (2004) 1–24.
[23] W.Y. Wang, Y. Ku, J. Membr. Sci. 282 (2006) 342–350.
[24] R. Wu, J. Qu, H. He, Y. Yu, Appl. Catal. B 48 (2004) 49–56.
[25] Y.S. Al-Degs, M.I. El-Barghouthi, A.H. El-Sheikh, G.M. Walker, Dyes Pigment 77 (2008) 16–23.
[26] X.H. Xu, W.F. Yao, Y. Zhang, A.Q. Zhou, Y. Hou, M. Wang, Acta Chim. Sinica 63 (2005) 5–10.
[27] L.Q. Jing, Y.C. Qu, B.Q. Wang, S.D. Li, B.J. Jiang, L.B. Yang, W. Fu, H.G. Fu, J.Z. Sun, Sol. Energy Mater. Sol. Cells 90 (2006) 1773–1787.
[28] D.W. Hwang, L.Y. Cha, J. Kim, H.G. Kim, S.W. Bae, J.S. Lee, Ind. Eng. Chem. Res. 42 (2003) 1184–1189.